Available online at www.sciencedirect.com
ScienceDirect
Journal of Sound and Vibration 300 (2007) 949–973
JOURNAL OF SOUND AND VIBRATION
www.elsevier.com/locate/jsvi

Sound transmission through curved aircraft panels with stringer and ring frame attachments

Bilong Liu[a,b,*], Leping Feng[a], Anders Nilsson[a]

[a]*MWL, Department of Aeronautical and Vehicle Engineering, KTH (The Royal Institute of Technology), SE-100 44, Sweden*
[b]*Institute of Acoustics, Chinese Academy of Sciences, 100080 Beijing, PR China*

Received 18 May 2005; received in revised form 11 September 2006; accepted 12 September 2006
Available online 13 November 2006

Abstract

A numerical approach based on a receptance method has been developed to evaluate the airborne sound insulation of aircraft panels with stringer and ring frame attachments. Theoretical predictions have been compared with laboratory measurements conducted on both model structures and aircraft panels. Certain parameters were varied in this study to gauge stiffener effects on sound transmission through the panel.

For large curved aircraft panels studied here, it was found that the ring frames have little influence on sound transmission loss in the frequency range of interest. However, the stringers may have considerable influence on the sound transmission loss. The stringer improves the sound transmission loss for a curved panel in the vicinity of the *ring frequency*, but may result in a potential deterioration above this frequency. In addition it was found that the sound transmission loss for the composite skin attached with composite stringers was lower than that of the metallic panel attached with metallic stringers. The results suggest that acoustical optimization design for the stringers is necessary to achieve improved airborne sound insulation for aircraft panels.

1. Introduction

Sound transmission through aircraft panels has received much attention recently. The four year EU project, Friendly Aircraft Cabin Environment, is an example showing such interest. Research on sound transmission through fuselage structures is commonly based on theoretical models of infinite cylindrical shells, with and without stiffening ribs [1–11]. Results show that two major dips dominate the description of sound transmission loss for a large diameter cylindrical shell. The first dip occurs at the cylinder ring frequency, where the interaction of bending forces and membrane forces in the shell leads to a minimum impedance of structure, and the second dip appears at the critical frequency, where the wavenumber of flexural waves in the panel are coincident with the wavenumber for acoustic pressure in air. When frequency increases to about twice the ring frequency, the shell behaves similarly to that of a flat panel.

*Corresponding author. Institute of Acoustics, Chinese Academy of Sciences, 100080 Beijing, PR China. Tel.: +86 10 82610737; fax: +86 10 62553898.
E-mail address: Liubl@mail.ioa.ac.cn (B. Liu).

0022-460X/$ - see front matter © 2006 Elsevier Ltd. All rights reserved.
doi:10.1016/j.jsv.2006.09.008

If a stiffener is attached to a flat panel, it is believed that this stiffener may deteriorate the sound transmission loss for the flat panel. The reason for this is that the wave reflections produced by the stiffener have wavenumber components of supersonic phase velocity that may propagate at frequencies below the uniform plate critical frequency. In short, these components increase the sub-critical radiation efficiency, thus decreasing the sound transmission loss, [12]. Increasing the complexity of the problem further, by taking the curvature into account, it is not straightforward to apply or modify flat stiffened panel theory to cylindrical shells. Koval [6,7] has developed a theoretical model to analyse the influence of ring frames and stringers on sound transmission through cylindrical shells. Numerical results indicate that the stiffeners have little effect on transmission loss below the ring frequency, but improve the transmission loss markedly above the ring frequency. Recently, Lee and Kim [13] developed a numerical approach based on a spatial harmonic technique to evaluate the sound transmission through periodically ring-stiffened cylindrical shells. Again, only numerical results with no qualifying measurement data were presented.

Although much theoretical work has been devoted to the sound transmission through cylindrical shells, the literature records no test data and theoretical models regarding the sound transmission through curved, finite aircraft shell panels with stringer and ring frame attachments. Due to the fact that only finite panels are possible for manufacture and for standard laboratory measurement, the sound insulation properties of individual finite panels are more relevant for study than that of the whole structure from the viewpoint of manufacture and measurement. Moreover, aircraft skins are stiffened by very strong ring frames, hence the situation of treating the response of individual panels independently is reasonable, whence it seems more realistic to model the skin as a finite panel rather than an infinite cylindrical shell. Generally, finite curved panels behave differently to infinite cylindrical shells; it is therefore necessary to make a comparison of the measurement and theoretical predictions for flat and curved panels, with and without stiffeners.

The receptance method is a dynamic flexibility technique which is commonly used in the free vibration analysis of stiffened structures. Wilken and Soedel [14,15] considered an exact and approximate method for studying the modal characteristics of ring-stiffened cylinders with the aid of a receptance method. Lin [16] investigated the forced vibration properties of stiffened flat plates, with an application to ship structures. In this article, however, a numerical approach based on receptance method has been developed to evaluate the airborne sound insulation of curved aircraft panels with stringer and ring frame attachments. Experimental data for simple aluminum panels and aircraft panels were collected by laboratory measurement to check the theoretical prediction. Stiffener cross-section parameters were varied to see how the stringer affects noise transmission.

2. Theory

A description of a theoretical model is presented in this section. The section begins with a theoretical model describing sound transmission loss through a flat rectangular panel before a description for curved panels is given.

2.1. Sound transmission through a flat, rectangular panel

Before considering a curved panel with stingers and frames, the basic theory of sound transmission through a flat, rectangular panel is briefly reviewed, for details, refer to [17]. Consider a simply supported, rectangular panel occupying the region $0 \leqslant x \leqslant a$, $0 \leqslant y \leqslant b$ within an infinite flat baffle, see Fig. 1. Sound is incident from one side and transmitted though the panel to other side. The differential equation governing the vibration of panel is given in Ref. [18]:

$$\left(D\nabla^4 - m_p\omega^2\right)w = 2p^i - 2p^r, \tag{1}$$

where w is the normal displacement of the panel, and the incident wave acting on the panel surface may be assumed as $p^i = \exp[\mathrm{j}(\omega t - k_x x - k_y y - k_z z)]$, p^r denotes the acoustic pressure radiated by the panel, $D = Eh^3/12(1-v^2)$ is the bending stiffness, E the Young's modulus, v the Poisson ratio, h the thickness of the panel, m_p the surface density of the panel, and j the imaginary unit $\sqrt{-1}$. The air density and sound speed are ρ_0 and c_0, respectively.

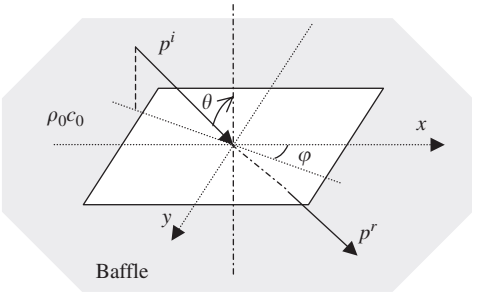

Fig. 1. Schematic of sound transmission through a rectangular panel.

Now, assume an eigenfunction for the simply supported panel as

$$\phi_{mn}(x,y) = \frac{2}{\sqrt{ab}} \sin\frac{m\pi x}{a} \sin\frac{n\pi y}{b}, \tag{2}$$

where m, n are positive integers.

Expanding the velocity with eigenfunctions in Eq. (2), and employing the orthogonal property of eigenfunctions yields the following relation:

$$\frac{m_p}{2j\omega}\left[\omega_{mn}^2(1+j\eta) - \omega^2\right] V_{mn} = P_{mn}^i - P_{mn}^r, \tag{3}$$

where V_{mn} is modal amplitude of panel velocity, η is panel material loss factor, ω_{mn} is the in vacuo resonant frequency of the panel, P_{mn}^i and P_{mn}^r are modal forces corresponding to external excitation and radiation, respectively. The eigenfrequencies and the modal forces in Eq. (3) are:

$$\omega_{mn}^2 = \frac{D}{m_p}\left[\left(\frac{m\pi}{a}\right)^2 + \left(\frac{n\pi}{b}\right)^2\right]^2, \tag{4}$$

$$P_{mn}^i = \int_0^b \int_0^a p^i \phi_{mn}(x,y)\,\mathrm{d}x\,\mathrm{d}y, \tag{5}$$

$$P_{mn}^r = \rho_0 c_0 \sum_{m',n'} Z_{m'n',mn} V_{m'n'}, \tag{6}$$

where $Z_{m'n',mn}$ is a dimensionless modal impedance describing the contributions from the modal velocity component. The real part of $Z_{m'n',mn}$, expressed as $\sigma_{m'n',mn}$, is modal radiation efficiency which is crucially related to sound power radiated by the panel. The imaginary part of $Z_{m'n',mn}$ is radiation reactance, describing virtual mass added on the vibrating surface. If the panel is assumed to be heavy in comparison with the fluid, this part has little effect on sound transmission loss and may be omitted in this calculation.

Furthermore, as presented in Refs. [18,19], non-diagonal elements of $\sigma m'n'mn$ have much less effect upon both the panel motion and the resultant sound transmission, therefore cross terms of modal radiation efficiency are neglected in subsequent panel response and sound radiation calculation.

Substituting Eqs. (5), (6) into Eq. (3), employing the orthogonal property and omitting radiation reactance, gives rise to modal response of the vibrating panel

$$V_{mn} = Y_{mn} P_{mn}^i, \tag{7}$$

where the modal admittance Y_{mn} is given by

$$Y_{mn} = \frac{2j\omega}{m_p}\left\{\omega_{mn}^2\left[1 + j\eta_{mn}^e\right] - \omega^2\right\}^{-1}, \tag{8}$$

and η_{mn}^{e} is the effective loss factor, defined by

$$\eta_{mn}^{e} = \eta + 2\frac{\rho_0 c_0}{m_p}\frac{\sigma_{mn}}{\omega_{mn}^2}\omega. \tag{9}$$

The transmitted power is then obtained, on neglecting cross terms of modal radiation efficiency, as

$$\Pi^t = \frac{1}{2}\mathrm{Re}\left\{\int_A p^r \cdot v * \mathrm{d}A\right\} = \frac{1}{2}\rho_0 c_0, \sum_{mn}\sigma_{mn}|Y_{mn}|^2\left|P_{mn}^i\right|^2, \tag{10}$$

where A is the surface area of the panel. Since the incident power is given by $\Pi^i = A\cos\theta/2\rho_0 c_0$, the transmission coefficient can be defined by

$$\tau(\theta,\varphi) = \Pi^t/\Pi^i = \frac{(\rho_0 c_0)^2}{\cos\theta}\sum_{mn}\sigma_{mn}|Y_{mn}|^2\left|P_{mn}^i\right|^2. \tag{11}$$

The transmission loss in a diffuse field is obtained by averaging over all incident angles

$$\mathrm{TL} = -10\log_{10}\frac{\int_0^{2\pi}\int_0^{\pi/2}\tau(\theta,\varphi)\sin\theta\cos\theta\,\mathrm{d}\theta\,\mathrm{d}\varphi}{\int_0^{2\pi}\int_0^{\pi/2}\sin\theta\cos\theta\,\mathrm{d}\theta\,\mathrm{d}\varphi}. \tag{12}$$

Note that the average of $\left|P_{mn}^i\right|^2$ over all incident angles is related to the modal radiation efficiency

$$\int_0^{2\pi}\int_0^{\pi/2}\left|P_{mn}^i\right|^2\sin\theta\,\mathrm{d}\theta\,\mathrm{d}\varphi = \frac{16\pi^2}{Ak^2}\sigma_{mn}. \tag{13}$$

Eq. (13) exhibits the close relation between P_{mn}^i and σ_{mn}, since the reciprocity principle requires that sound radiation must be governed equivalently to the variables involved in the original forcing field.

The combination of Eqs. (11), (12) and (13), gives rise to an expression for sound transmission loss

$$\mathrm{TL} = -10\log\frac{4\pi(\rho_0 c_0)^2}{Ak^2}\sum_{mn}|Y_{mn}|^2\sigma_{mn}^2. \tag{14}$$

In Eq. (14), the modal radiation efficiency σ_{mn} for a simply supported panel has been obtained previously by an approach due to Wallace [20]. In practice, however, the fuselage panel is never ideally simply supported. There is always a constraint against rotation along the plate edges. Since no exact solution exists for a plate clamped along all edges, to predict the radiation efficiency for such cases various alternative approaches have been made available, see Ref. [20]. In the present work, the modal radiation ratio of clamped plates has been evaluated by a method based on the modal radiation efficiency for simply supported plates. This is possible since modal shapes for a clamped plate may be estimated rather accurately by considering an equivalent simply supported plate with virtual dimensions depending on the modal order. As shown in Ref. [21], the normalized eigenfunction of clamped plate may be approximated by the following expression:

$$\phi_{mn}^c(x,y) = \frac{2}{\sqrt{a_{mn}b_{mn}}}\sin\frac{m\pi x}{a_{mn}}\sin\frac{n\pi y}{b_{mn}}, \tag{15}$$

where the virtual panel dimensions are given by

$$a_{mn} = \frac{m}{m+\Delta m}a, \quad b_{mn} = \frac{n}{n+\Delta n}b, \tag{16a–16b}$$

$$\Delta m = \left[\left(\frac{na}{mb}\right)^2 + 2\right]^{-1} + \left(\frac{0.017}{m}\right), \quad \Delta n = \left[\left(\frac{mb}{na}\right)^2 + 2\right]^{-1} + \left(\frac{0.017}{n}\right). \tag{16c–16d}$$

By implementing corresponding corrections for the calculation of modal radiation efficiency and the modal admittance, the sound transmission loss of the rectangular panel with clamped edges can be estimated by using Eq. (14). Strictly speaking, the approach for the panel with clamped boundary conditions is not correct since the modes assumed in Eq. (15) are not orthogonal. However, the modal cross terms can be omitted due to

their trivial influence on the panel motion and the resultant sound transmission, and therefore a good approximation for this approach can be expected.

2.2. Sound transmission through a curved, rectangular panel

Now consider a simply supported, slightly curved rectangular panel occupying the region $0 \leqslant x \leqslant a$ and $0 \leqslant y \leqslant b$ within an infinite flat baffle, see Fig. 2. Sound is incident from one side and transmitted though the panel. The panel vibration in this study may be conveniently described by Donnell–Mushtari–Vlasov equations [22]

$$D\nabla^4 w + \nabla_k^2 \zeta - m_p \omega^2 w = 2p^i - 2p^r, \tag{15a}$$

$$Eh\nabla_k^2 w - \nabla^4 \zeta = 0, \tag{15b}$$

where w represents the transverse displacement of the curved panel, whilst the function ζ is in general known as *Airy's stress* function and was introduced to eliminate the coupled in-plane displacements [22], r is radial of the curvature, and second-order operator $\nabla_k^2(.) = \partial^2(.)/r\partial x^2$.

Again, expanding all variables in Eq. (15) with the eigenfunctions in Eq. (2), and following the similar procedure presented in Section 2.1, the function ζ in Eqs. (15a) and (15b) can be eliminated, the modal response of the curved, rectangular panel is therefore obtained

$$V_{mn} = Y_{c,mn} P_{mn}^i, \tag{16}$$

where represents the modal admittance of the curved, rectangular panel, given by

$$Y_{c,mn} = \frac{\mathrm{j}\omega}{m_p} \left\{ \omega_{c,mn}^2 \left[1 + \mathrm{j}\eta_{mn}^e \right] - \omega^2 \right\}^{-1}, \tag{17a}$$

where the corresponding resonant frequency of the curved panel $\omega_{c,mn}$ is given by

$$\omega_{c,mn}^2 = \frac{D}{m_p} \left[\left(\frac{m\pi}{a} \right)^2 + \left(\frac{n\pi}{b} \right)^2 \right]^2 + \frac{Eh}{r^2 m_p} \left[1 + \left(\frac{na}{mb} \right)^2 \right]^{-2}. \tag{17b}$$

Therefore an expression for the sound transmission through the curved, rectangular panel is given by

$$\mathrm{TL} = -10\log_{10} \frac{4\pi \left(\rho_0 c_0 \right)^2}{Ak^2} \sum_{mn} \left| Y_{c,mn} \right|^2 \sigma_{mn}^2. \tag{18}$$

In Eq. (18), the modal radiation efficiency of the curved, rectangular panel is assumed to be that of a flat, rectangular panel of similar dimensions. If the curved panel is confined to the scope of slightly curved, shallow shells, then the difference of modal radiation efficiency between a curved and flat panel is small and can be neglected, Ref. [23].

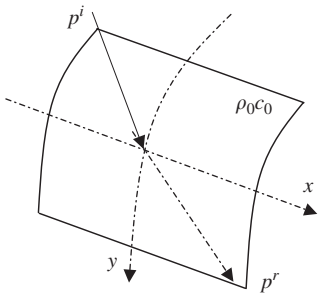

Fig. 2. Schematic of sound transmission through a curved, rectangular panel.

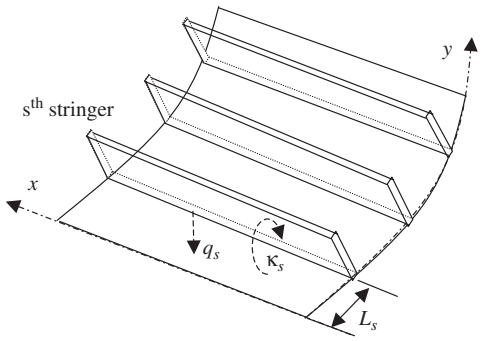

Fig. 3. A stiffened curved, rectangular panel.

2.3. Sound transmission through a curved rectangular panel with stringer attachments

Consider a simply supported cylindrical panel with axial stiffener attachments, see Fig. 3. To analyse the bending modes of a curved panel with stiffening stringers, it is reasonable to assume that the stiffeners experience radial and torsional motion only, and that the modal receptances of a cylindrical shell may be defined by its bending modes only. It is also assumed that the system is joined along middle surfaces, thus the eccentric effects are neglected, i.e. the cross-section of each stiffener is not symmetric to the middle surface of the shell. In reality, the ring may be joined to the panel either above or below. This influence is generally small but has been investigated in references [14,15].

The Donnell–Mushtari–Vlasov equations governing the vibration of curved panel under the conditions of above assumptions are given by

$$D\nabla^4 w + \nabla_k^2 \zeta - m_p \omega^2 w = 2p^i - 2p^r - \sum_{s=1}^{S} q_s \delta(y - L_s) - \sum_{s=1}^{S} \kappa_s \delta'(y - L_s), \tag{19a}$$

$$Eh\nabla_k^2 w - \nabla^4 \zeta = 0, \tag{19b}$$

where L_s represents the distance between sth stringers and boundary, q_s, κ_s represents the radial force and moment exerted on the shell wall exerted by stringers, respectively, and S represents the total number of stringers.

An eigenfunction describing the simply supported panel deflection is again assumed as

$$\phi_m(x)\phi_n(y) = \frac{2}{\sqrt{ab}} \sin\frac{m\pi x}{a} \sin\frac{n\pi y}{b}. \tag{20}$$

Expanding w and ζ with the eigenfunction in Eq. (20) and by employing the orthogonal property yields an equation for the modal amplitude of the panel velocity

$$\frac{m_p}{2\mathrm{j}\omega}\left\{\omega_{c,mn}^2(1 + \mathrm{j}\eta_{mn}^e) - \omega^2\right\} V_{mn} = P_{mn}^i - \sum_{s=1}^{S} Q_s \phi_n(L_s) - \sum_{s=1}^{S} M_s \phi_n'(L_s), \tag{21}$$

where $Q_s = \int_0^b q_s \phi(x)\,\mathrm{d}y$, $M_s = \int_0^b \kappa_s \phi(x)\,\mathrm{d}y$ are the modal coupling force and moment at the sth stringer/shell interface.

Rewriting Eq. (21) as

$$V_{mn} = Y_{c,mn}\left(P_{mn}^i - \left[\boldsymbol{\varphi}_n, \quad \boldsymbol{\varphi}_n'\right]\begin{bmatrix}\mathbf{Q}\\ \mathbf{M}\end{bmatrix}\right), \tag{22}$$

where

$$\mathbf{Q} = \begin{bmatrix} Q_1 & Q_2 & \cdots & Q_S \end{bmatrix}^{\mathrm{T}}, \; M = \begin{bmatrix} M_1 & M_2 & \cdots & M_S \end{bmatrix}^{\mathrm{T}}, \tag{23}$$

$$\boldsymbol{\varphi}_n = \left[\begin{array}{cccccc} \phi_n(L_{s1}) & \phi_n(L_{s2}) & \phi_n(L_{s3}) & \ldots & \phi_n(L_{sS}) \end{array}\right], \tag{24}$$

$$\boldsymbol{\varphi}_n^{'} = \left[\begin{array}{cccccc} \phi_n^{'}(L_{s1}) & \phi_n^{'}(L_{s2}) & \phi_n^{'}(L_{s3}) & \ldots & \phi_n^{'}(L_{sS}) \end{array}\right]. \tag{25}$$

Now recalling the governing equations of the stiffener flexural and torsional displacement given in Ref. [24]

$$\left(D_s \mathrm{d}^4/\mathrm{d}x^4 - m_s\omega^2\right) w_s = q_s, \tag{26}$$

$$\left(T_s \mathrm{d}^2/\mathrm{d}x^2 - EI_w \mathrm{d}^4/\mathrm{d}x^4 + \rho_s I_p \omega^2\right)\theta_s = \kappa_s, \tag{27}$$

where D_s and T_s are, respectively, the bending and torsional stiffness of the beam stiffener, I_w is the warping constant of the stiffener, m_s is the mass per unit length of the stringer, η_s is loss factor of the stiffeners, I_p is the polar moment of inertia for the beam.

According to Eqs. (26) and (27), the corresponding line input modal receptances of the stringer due to the normal force and moment are

$$\beta_m^Q = \frac{1}{m_s\left[\omega_{Qm}^2(1+\mathrm{j}\eta_s) - \omega^2\right]}, \tag{28}$$

$$\beta_m^M = -\frac{1}{\rho I_s\left[\omega_{Mm}^2(1+\mathrm{j}\eta_s) - \omega^2\right]}, \tag{29}$$

where ω_{Qm} and $\omega_{Mm}$are the eigenfrequencies of the stiffener for bending modes and torsional modes, respectively, written as

$$\omega_{Qm}^2 = \frac{D_s}{m_s}\left(\frac{m\pi}{a}\right)^4, \tag{30}$$

$$\omega_{Tm}^2 = \frac{T_s}{\rho I_s}\left(\frac{m\pi}{a}\right)^2 - \frac{EI_w}{\rho I_s}\left(\frac{m\pi}{a}\right)^4. \tag{31}$$

By using the definition of receptance and Eq. (24), yields

$$\beta_m^Q = \frac{\sum\limits_n V_{mn}\phi_n(L_s)}{\mathrm{j}\omega Q_s} = \frac{1}{\mathrm{j}\omega Q_s}\sum_n\left(P_{mn}^i - \left[\begin{array}{cc}\boldsymbol{\varphi}_n, & \boldsymbol{\varphi}_n^{'}\end{array}\right]\left[\begin{array}{c}\mathbf{Q}\\ \mathbf{M}\end{array}\right]\right) Y_{c,mn}\phi_n(L_s), \tag{32}$$

$$\beta_m^M = \frac{\sum\limits_n V_{mn}\phi_n(L_s)}{\mathrm{j}\omega M_s} = \frac{1}{\mathrm{j}\omega M_s}\sum_n\left(P_{mn}^i - \left[\begin{array}{cc}\boldsymbol{\varphi}_n, & \boldsymbol{\varphi}_n^{'}\end{array}\right]\left[\begin{array}{c}\mathbf{Q}\\ \mathbf{M}\end{array}\right]\right) Y_{c,mn}\phi_n^{'}(L_s). \tag{33}$$

The combination of Eqs. (32) and (33), yields a matrix equation whose entries are themselves infinite sums

$$\left[\begin{array}{cc}\mathbf{A} & \mathbf{B}\\ \mathbf{C} & \mathbf{D}\end{array}\right]\left[\begin{array}{c}\mathbf{Q}\\ \mathbf{M}\end{array}\right] = \sum_n P_{mn}^i Y_{c,mn}\left[\begin{array}{c}\boldsymbol{\varphi}_n^{\mathrm{T}}\\ \boldsymbol{\varphi}_n^{'\mathrm{T}}\end{array}\right], \tag{34}$$

where $\boldsymbol{\varphi}_n^{\mathrm{T}}$ and $\boldsymbol{\varphi}_n^{'\mathrm{T}}$ denote the transposes of matrices $\boldsymbol{\varphi}_n$ and $\boldsymbol{\varphi}_n'$, and the matrix elements are

$$A_{s1,s2} = \begin{cases} \sum\limits_n Y_{mn}\phi_n(L_{s1})\phi_n(L_{s2}), & s1 \neq s2, \\ \sum\limits_n Y_{mn}\phi_n(L_{s1})\phi_n(L_{s2}) + \mathrm{j}\omega\beta_m^Q, & s1 = s2, \end{cases}$$

$$B_{s1,s2} = \sum_n Y_{mn}\phi_n(L_{s1})\phi_n^{'}(L_{s2}), \quad C_{s1,s2} = \sum_n Y_{mn}\phi_n^{'}(L_{s1})\phi_n(L_{s2}),$$

$$D_{s1,s2} = \begin{cases} \sum_n Y_{mn}\phi'_n(L_{s1})\phi'_n(L_{s2}), & s1 \neq s2, \\ \sum_n Y_{mn}\phi'_n(L_{s1})\phi'_n(L_{s2}) + \mathrm{j}\omega\beta^M_m, & s1 = s2, \end{cases}$$

$$s1, s2 = 1, 2, 3, \ldots, S. \tag{35a-35e}$$

Combining Eqs. (22) and (34), yields the modal response of the curved panel

$$V_{mn} = Y_{mn}\left(P^i_{mn} - \sum_{n'} P^i_{mn'} Y_{c,mn'} \Phi_{n'}\right), \tag{36}$$

where

$$\mathbf{\Phi}_{n'} = \begin{bmatrix} \boldsymbol{\varphi}_n & \boldsymbol{\varphi}'_n \end{bmatrix} \begin{bmatrix} \mathbf{A} & \mathbf{B} \\ \mathbf{C} & \mathbf{D} \end{bmatrix}^{-1} \begin{bmatrix} \boldsymbol{\varphi}^{\mathrm{T}}_{n'} \\ \boldsymbol{\varphi}'^{\mathrm{T}}_{n'} \end{bmatrix}. \tag{37}$$

The method above used to derive Eq. (36) extends the approach due to Lin [16], where a derivation of the response for a stiffened flat plate under mechanical force excitation is described.

Once the response of the panel is derived, following the same procedure in the preceding section, neglecting the cross terms of modal radiation resistance, an expression for sound transmission loss through the curved panel with stringers is obtained, Appendix A,

$$\mathrm{TL} = -10\log_{10}\frac{4\pi(\rho_0 c_0)^2}{Ak^2}\sum_{mn} Y^2_{c,mn}\sigma_{mn}\left(\sigma_{mn} - 2\sigma_{mn}\mathrm{Re}\{Y_{c,mn}\mathbf{\Phi}_n\} + \sum_{n'}\sigma_{mn'}\left|Y_{c,mn'}\mathbf{\Phi}_{n'}\right|^2\right). \tag{38}$$

In Eq. (38), the second and third terms in the brackets represents the contribution from the stringers. Note that if these terms are set to zero, then the equation is same as the expression of the sound transmission loss for a curved panel without axial stiffeners, Eq. (18).

2.4. Sound transmission through a curved, rectangular panel with ring frame attachments

Now consider a simply supported cylindrical panel with stiffeners in the circumferential direction, see Fig. 4. The corresponding equations governing the vibration of curved panel with ring frame stiffeners under the assumptions in Section 2.3 are given by

$$D\nabla^4 w + \nabla^2_k \zeta - m_p\omega^2 w = 2p^i - 2p^r - \sum_{t=1}^{T} q_t\delta(x - L_t) - \sum_{t=1}^{T}\kappa_t\delta'(x - L_t), \tag{39a}$$

$$Eh\nabla^2_k w - \nabla^4\zeta = 0, \tag{39b}$$

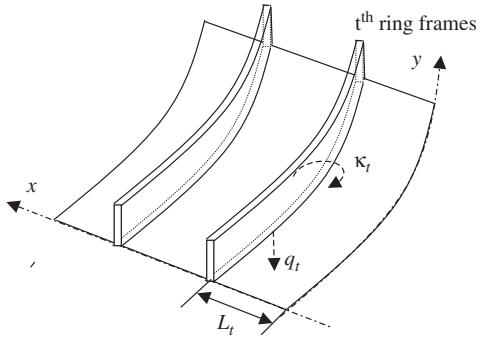

Fig. 4. A curved, rectangular panel with circumferential stiffeners.

where L_t represents the distance between tth ring frame and boundary , q_t and κ_t represent the radial force and moment exerted on the shell wall by stiffeners, respectively, and T denotes the total number of ring frame stiffeners.

If there is no circumferential force and the circumferential inertia term may be assumed to be negligible, then the governing equations of the radial and torsional motion of a circumferential stiffener are given in Refs. [22,25]

$$\left[D_r\left(\mathrm{d}^4/\mathrm{d}y^4 + 2\mathrm{d}^2/r^2\mathrm{d}y^2 + 1/r^4\right) - m_r\omega^2\right]w_r = q_t, \tag{40}$$

$$\left(T_r\mathrm{d}^2/\mathrm{d}y^2 - E_r\bar{I}/r^2 + \rho_r I_{pr}\omega^2\right)\theta_r = \kappa_t, \tag{41}$$

where w_r and θ_r are radial deflection and torsional angle, respectively, D_r and κ_r are respectively the bending and torsional stiffness of the ring, m_r is the ring mass per unit length, $\bar{I}$ is the moment of the inertia of the cross-section about axes parallel to the radial direction and I_{pr} is the polar moment of inertia of the ring cross-section.

According to Eqs. (40) and (41), the line input modal receptances of the ring stiffener due to the normal force and torsional moment are obtained

$$\beta_n^Q = \frac{1}{m_r\left[\omega_{Qn}^2(1+\mathrm{j}\eta_r) - \omega^2\right]}, \tag{42}$$

$$\beta_n^M = -\frac{1}{\rho_r I_{pr}\left[\omega_{Mn}^2(1+\mathrm{j}\eta_r) - \omega^2\right]}, \tag{43}$$

respectively, where η_r is loss factor of the ring stiffener, ω_{Qn} and ω_{Mn} is the eigenfrequency of the ring stringer for bending modes and torsional modes, given by

$$\omega_{Qn}^2 = \frac{D_r}{m_r}\left[\left(\frac{n\pi}{b}\right)^4 - \frac{2}{r}\left(\frac{n\pi}{b}\right)^2 + \frac{1}{r^4}\right], \tag{44}$$

$$\omega_{Mn}^2 = \frac{1}{\rho I_{pr}}\left[\frac{E\bar{I}}{r^2} + T_r\left(\frac{n\pi}{b}\right)^2\right]. \tag{45}$$

Following a similar procedure in Section 2.3, neglecting the cross terms for modal radiation efficiency, an expression for sound transmission through the curved panel with attached ring frames is obtained:

$$\mathrm{TL} = -10\log\frac{4\pi\left(\rho_0 c_0\right)^2}{Ak^2}\sum_{mn} Y_{c,mn}^2\sigma_{mn}\left(\sigma_{mn} - 2\sigma_{mn}\mathrm{Re}\left\{Y_{c,mn}\boldsymbol{\Phi}_m\right\} + \sum_{m'}\sigma_{m'n}\left|Y_{c,m'n}\boldsymbol{\Phi}_{m'}\right|\right), \tag{46}$$

where

$$\boldsymbol{\Phi}_{m'} = \begin{bmatrix}\boldsymbol{\varphi}_m & \boldsymbol{\varphi}'_m\end{bmatrix}\begin{bmatrix}\mathbf{A}^r & \mathbf{B}^r\\ \mathbf{C}^r & \mathbf{D}^r\end{bmatrix}^{-1}\begin{bmatrix}\boldsymbol{\varphi}_{m'}^{\mathrm{T}}\\ \boldsymbol{\varphi}'^{\mathrm{T}}_{m'}\end{bmatrix} \tag{47}$$

and the matrix elements are

$$A_{t1,t2}^r = \begin{cases}\sum\limits_m Y_{mn}\phi_m(L_{t1})\phi_m(L_{t2}), & t1 \neq t2,\\ \sum\limits_m Y_{mn}\phi_m(L_{t1})\phi_m(L_{t2}) + \mathrm{j}\omega\beta_n^Q, & t1 = t2,\end{cases}$$

$$B_{t1,t2}^r = \sum_m Y_{mn}\phi_m(L_{t1})\phi'_m(L_{t2}),\quad C_{t1,t2}^r = \sum_m Y_{mn}\phi'_m(L_{t1})\phi_m(L_{t2}),$$

$$D^r_{t1,t2} = \begin{cases} \sum_m Y_{mn}\phi'_m(L_{t1})\phi'_m(L_{t2}), & t1 \neq t2, \\ \sum_m Y_{mn}\phi'_m(L_{t1})\phi'_m(L_{t2}) + \mathrm{j}\omega\beta^M_n, & t1 = t2, \end{cases}$$

$$t1, t2 = 1, 2, 3, \ldots, T. \tag{48a–e}$$

2.5. Sound transmission through a curved rectangular panel with stringer and ring frame attachments

The differential equations governing the vibration of curved panel with attached stiffeners in axial and circumferential direction (Fig. 5) under the conditions of assumptions in Section 2.3 are given by

$$D\nabla^4 w + \nabla_k^2\zeta - m_p\omega^2 w = 2p^i - 2p^r - \sum_{s=1}^{S} q_s\delta(y - L_s) - \sum_{s=1}^{S} \kappa_s\delta'(y - L_s) - \sum_{t=1}^{T} q_t\delta(x - L_t) - \sum_{t=1}^{T} \kappa_t\delta'(x - L_t), \tag{49a}$$

$$Eh\nabla_k^2 w - \nabla^4\zeta = 0. \tag{49b}$$

Following the procedure outlined in Sections 2.3 and 2.4, and neglecting the cross term of modal radiation efficiency, an expression for sound transmission through the curved panel with stringers and ring frames is obtained.

$$\mathrm{TL} = -10\log_{10}\frac{4\pi(\rho_0 c_0)^2}{Ak^2}\sum_{mn} Y^2_{c,mn}\sigma_{mn}\left(\sigma_{mn} - 2\sigma_{mn}\mathrm{Re}\left\{Y_{c,mn}\boldsymbol{\Phi}^s_n\right\} - 2\sigma_{mn}\mathrm{Re}\left\{Y_{c,mn}\boldsymbol{\Phi}^r_m\right\} + 2\sigma_{mn}Y^2_{c,mn}\mathrm{Re}\left\{\boldsymbol{\Phi}^s_n\boldsymbol{\Phi}^r_m\right\} + \sum_{m'}\sigma_{m'n}\left|Y_{c,m'n}\boldsymbol{\Phi}^r_{m'}\right|^2 + \sum_{n'}\sigma_{mn'}\left|Y_{c,mn'}\boldsymbol{\Phi}^s_{n'}\right|^2\right). \tag{50}$$

where

$$\boldsymbol{\Phi}^r_m = \begin{bmatrix} \boldsymbol{\varphi}_n & \boldsymbol{\varphi}'_n & \boldsymbol{\varphi}_m & \boldsymbol{\varphi}'_m \end{bmatrix} \begin{bmatrix} \mathbf{A} & \mathbf{B} & \mathbf{E}^1 & \mathbf{E}^2 \\ \mathbf{C} & \mathbf{D} & \mathbf{E}^3 & \mathbf{E}^4 \\ \mathbf{F}^1 & \mathbf{F}^2 & \mathbf{A}^r & \mathbf{B}^r \\ \mathbf{F}^3 & \mathbf{F}^4 & \mathbf{C}^r & \mathbf{D}^r \end{bmatrix}^{-1} \begin{bmatrix} \boldsymbol{\varphi}^{\mathrm{T}}_n \\ \boldsymbol{\varphi}'^{\mathrm{T}}_n \\ 0 \\ 0 \end{bmatrix}, \tag{51}$$

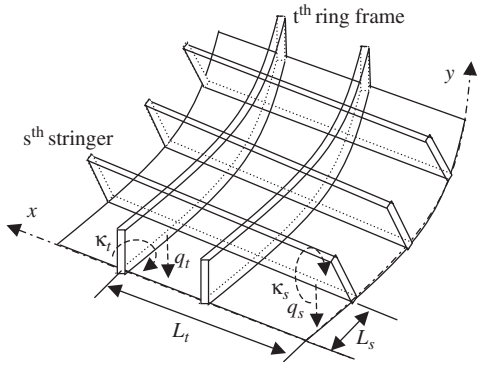

Fig. 5. A curved, rectangular panel with axial and circumferential stiffeners.

$$\mathbf{\Phi}_m^r = \begin{bmatrix} \boldsymbol{\varphi}_n & \boldsymbol{\varphi}'_n & \boldsymbol{\varphi}_m & \boldsymbol{\varphi}'_m \end{bmatrix} \begin{bmatrix} \mathbf{A} & \mathbf{B} & \mathbf{E}^1 & \mathbf{E}^2 \\ \mathbf{C} & \mathbf{D} & \mathbf{E}^3 & \mathbf{E}^4 \\ \mathbf{F}^1 & \mathbf{F}^2 & \mathbf{A}^r & \mathbf{B}^r \\ \mathbf{F}^3 & \mathbf{F}^4 & \mathbf{C}^r & \mathbf{D}^r \end{bmatrix}^{-1} \begin{bmatrix} 0 \\ 0 \\ \boldsymbol{\varphi}_m^{\mathrm{T}} \\ \boldsymbol{\varphi}'^{\mathrm{T}}_m \end{bmatrix}. \tag{52}$$

In Eq. (51) and (52) the entries that differ from those given in Sections 2.3 and 2.4 are given by

$$E^1_{s,t} = \sum_m Y_{c,mn}\phi_n(L_s)\phi_m(L_t), \quad E^2_{s,t} = \sum_m Y_{c,mn}\phi_n(L_s)\phi'_m(L_t),$$

$$E^3_{s,t} = \sum_m Y_{c,mn}\phi'_n(L_s)\phi_m(L_t), \quad E^4_{s,t} = \sum_m Y_{c,mn}\phi'_n(L_s)\phi'_m(L_t),$$

$$F^1_{t,s} = \sum_n Y_{c,mn}\phi_n(L_s)\phi_m(L_t), \quad F^2_{t,s} = \sum_n Y_{c,mn}\phi_n(L_s)\phi'_m(L_t),$$

$$F^3_{t,s} = \sum_n Y_{c,mn}\phi'_n(L_s)\phi_m(L_t), \quad F^4_{t,s} = \sum_n Y_{c,mn}\phi'_n(L_s)\phi'_m(L_t),$$

$$s = 1, 2, 3, \ldots, S, \quad t = 1, 2, 3 \ldots, T. \tag{53a–53j}$$

3. Comparison of measurement and theoretical prediction

A detailed description of measurement data and theoretical prediction is given in this section. The section begins with a description of experimental set up and test samples used for sound transmission loss measurement.

3.1. Test set up and test sample description

The sound transmission losses of the panels are measured according to standard ISO 15186-1:2000 [26] with an intensity method, see Fig. 6. The test sample is mounted in between a reverberation room and an anechoic room. The reverberation room (6.21 m × 7.86 m × 5.05 m) is used as the source room and a rotating microphone is used to measure average sound pressure level. The anechoic room (7 m × 5.95 m × 5.8 m, cut off frequency 80 Hz) is used as the receiving room and the average sound intensity level over the surface of the sample is measured by using a scan method. The laboratory facilities available to the authors at Marcus

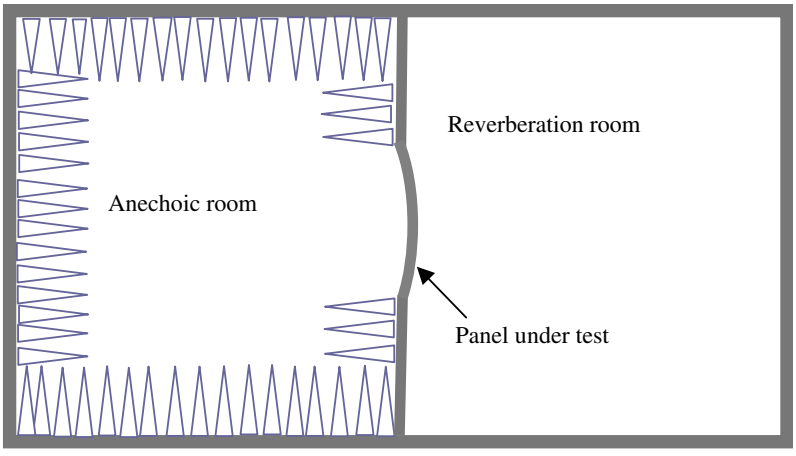

Fig. 6. Set-up for transmission loss measurements.

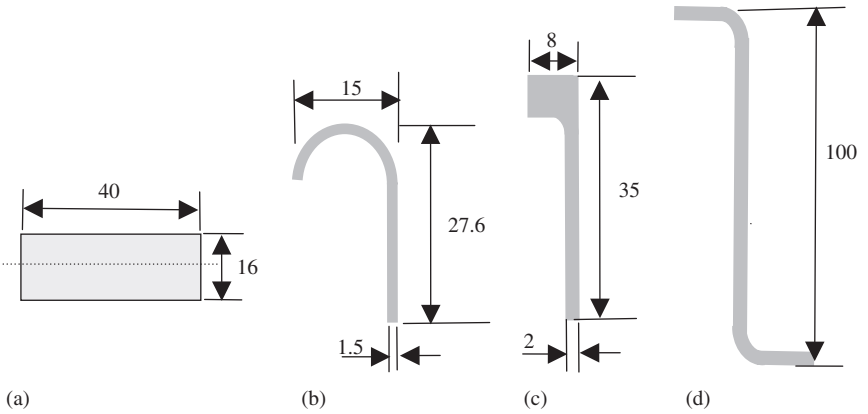

Fig. 7. Schematic of stiffener cross-section, (a) ring ribs for Panel F, (b) stringers for Panel G, (c) stringers for Panel H, (d) ring frames for Panel G and H (mm-scale). The feet of the stringer are included in the equivalent thickness of the panel, and therefore not illustrated in this diagram.

Table 1
Panels used in measurement

Panel	Material	Radius (m)	Size (m^2)	Skin area density (kg/m^2)	Young's modulus (N/m^2)	Stiffener	Loss factor
A	Aluminum	∞	0.8×0.87	2.7	6.85E+10	no	0.01
B	Aluminum	4	0.87×0.91	2.7	6.85E+10	no	
C	Aluminum	1	0.87×0.95	2.7	6.85E+10	no	
D	Aluminum	1	0.87×0.95	2.7	6.85E+10	yes	
E	Composite	∞	0.535×1.25	4.0	3.25E+10	no	0.15
F	Composite	∞	0.535×1.25	4.9	3.25E+10	Yes	see Table 2
G	Metallic	2	1.67×2.2	5.4	6.85E+10	Yes	
H	Composite	2	1.67×2.2	5.4	3.25E+10	yes	

Fig. 8. Test arrangement for a home-made panel (Panel D), (left), side of reverberation room, (right), side of anechoic room.

Wallenberg Laboratory for Sound and Vibration Research (MWL), KTH, Sweden are well equipped for sound transmission loss experiments giving repeatability for measurements less than 0.5 dB throughout the given frequency range. The intensity sound reduction index or sound transmission loss is calculated according to the standard as

$$\mathrm{TL}_I = L_{Pi} - 6 - (L_{In} + 10\log(S_m/S)), \tag{54}$$

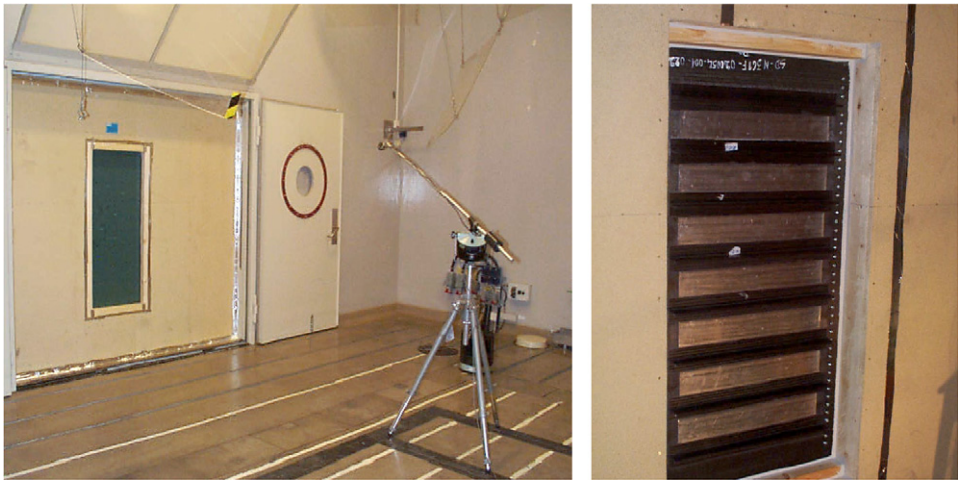

Fig. 9. Test arrangement for a small aircraft panel (Panel F), (left), side of reverberation room, (right), side of anechoic room.

Fig. 10. Test arrangement for a large metallic panel (Panel G), (left), side of reverberation room, (right), side of anechoic room.

Table 2
Loss factors for Panels F, G and H

Frequency (Hz)	100	125	160	200	250	315	400	500	630	800	⩾1 k
Panel F	0.13	0.11	0.06	0.07	0.063	0.043	0.024	0.021	0.02	0.02	0.015
Panel G	0.11	0.07	0.05	0.04	0.04	0.04	0.03	0.03	0.02	0.02	0.015
Panel H	0.12	0.12	0.07	0.06	0.06	0.04	0.03	0.03	0.02	0.02	0.015

*The loss factors below 1 kHz are obtained by measurement, and above are estimated.

where L_{Pi} is the averaged sound pressure level in the source room and L_{In} is the averaged sound intensity level over the panel surface measured in the anechoic room, S_m is the measurement area and S is the area of the test specimen. For the measurements in this study, $S_m = S$ (Fig. 7).

Eight panels shown in Table 1 are used in the measurements. In Table 1, Panel A, B and C are aluminum panels with similar physical parameters but with different curvatures chosen to check the influence of curvature effects. Panel D is same as Panel C but with two steel ribs attached, Fig. 8. Panel E is a small composite aircraft panel without stringer. Panel F is the same but stiffened with densely-arranged stringers and is heavily damped, Fig. 9. Panel G and H are large aircraft panels in which Panel G is made from

Table 3
General parameters of stiffeners

Panel	Description	Weight per stiffener (kg)	Stiffener thickness (mm)	Stiffener height (mm)	Density (kg/m^3)	Young's modulus (N/m^2)	Loss factor
D	Ring Rib	5	40	16	7800	2.1E+11	0.015
F	Stringer	0.1	2	35	1620	3.25E+10	
G	Stringer	0.5	1.5	28	2700	6.85E+10	
	Ring frame	1.1	1.5	100	2700	6.85E+10	
H	Stringer	0.5	2	35	1620	3.25E+10	
	Ring frame	1.1	3	100	1620	3.25E+10	

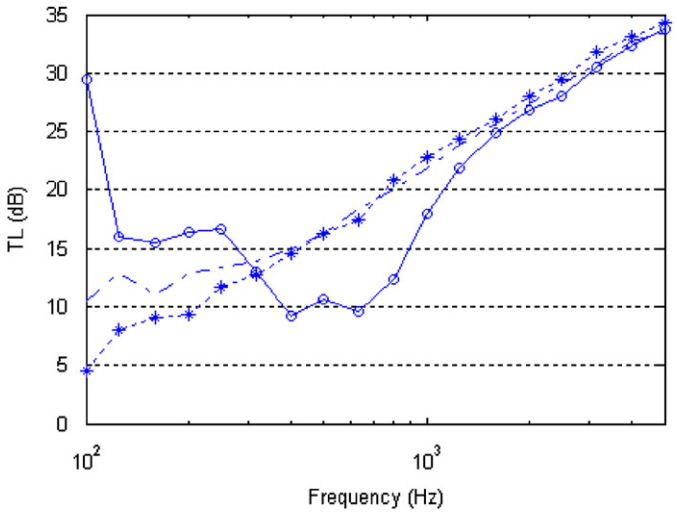

Fig. 11. Measured TL for the panels with different curvature: ------ Panel A, flat; ---*--- Panel B, r = 4; —○— Panel C, $r = 1$.

aluminum and Panel H is a composite with same weight and similar structural arrangement. Panels G and H are stiffened with stringers and ring frames and heavily damped at the concave side, Fig. 10. The stringers cover around 60% of the panel, the remainder without stringers are designed for allocation of windows. Therefore, two areas, stringer area and window area, may be classified for Panels G and H. It must be noted that the panel thickness for stringer area and window area are not the same. To avoid the complexity of the prediction model, the equivalent thicknesses, for example, 2 mm for Panel G and 3.3 mm for Panel H, are adopted in the calculation.

Table 2 shows the measured loss factors when the panels are installed. In the measurements, the panels are clamped at the edges. The general information of the stiffeners are shown in Table 3 and Fig. 7, where the feet of the stringers are included in the panel skin, and therefore not illustrated in Fig. 7. Also, it is worthwhile to note that the ring ribs for Panel D are wide, heavy and quite stiff in comparison with a skin panel.

3.1. Comparison of measured and predicted sound transmission loss

3.1.1. Curvature effect

Firstly Fig. 11 shows the test results for three panels with the same physical parameters but different curvature. One clear conclusion from Fig. 11 is that the curvature, although rather shallow, may result in significant influence on sound transmission loss. It is evident that the curvature reduces sound transmission around the ring frequency of the corresponding panel ($f_r = \sqrt{E/\rho(1-v^2)}\big/2\pi r$). The most effected frequencies, however, are located slightly below rather than exactly at the ring frequency. When the frequency is increased to about twice to that of the ring frequency, the sound transmission loss of the curved

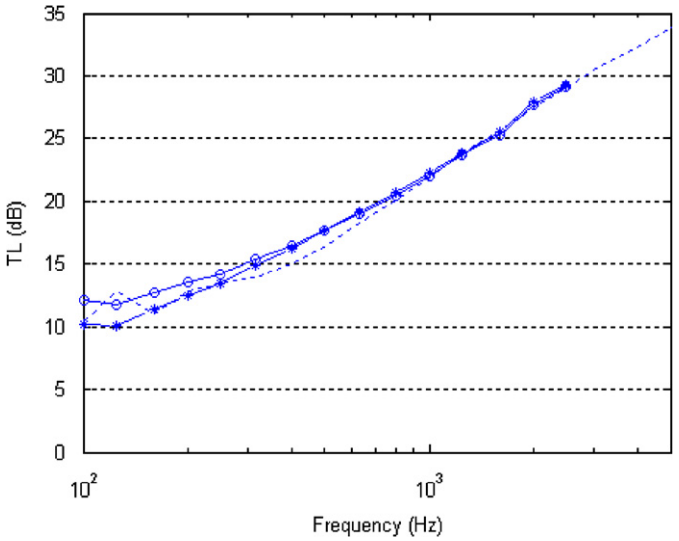

Fig. 12. Measured and predicted TL for Panel A: ------ Measurement; —○— Cal., clamped; ---*--- Cal., simply supported.

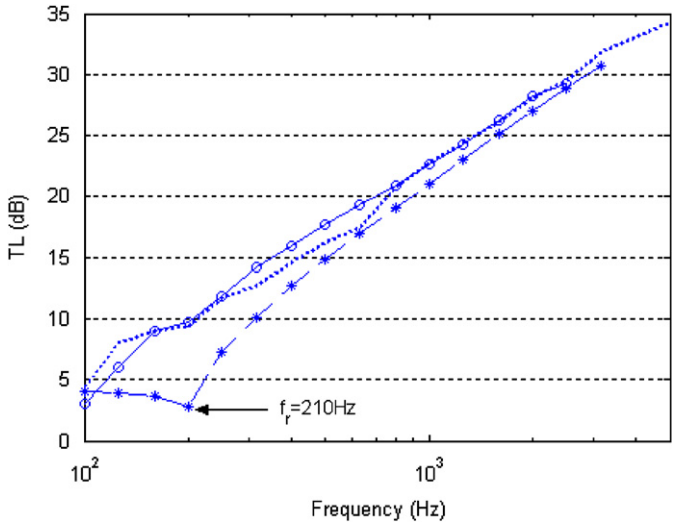

Fig. 13. Measured and predicted TL for Panel B: ------ Measurement; —○— Cal., clamped; ---*--- Cal., infinite model Ref. [3].

panel agrees with that of the equivalent flat panel, whereas far below the ring frequency, the finite curved panel yields much better sound insulation properties than the corresponding flat panel.

The comparison of the theoretical prediction and test are also shown in Figs. 12–14, where the predictions from infinite model of the curved panels are also plotted according to Ref. [3]. It is found that the calculation from the finite panel model with and without clamped correction agree well with the test result, showing that the boundary effects for the panels studied are not obvious, see Fig. 12. The prediction also shows that the infinite model can provide good agreement with the test results above about twice the ring frequency; however, the finite model failed to provide good agreement close to and below the ring frequency. For the prediction from the infinite model, the sound transmission loss is underestimated far below the ring frequency, and moreover the least beneficial sound transmission loss always appeared at the ring frequency, whereas the measurement and the prediction from the finite model show this dip is located below the ring frequency.

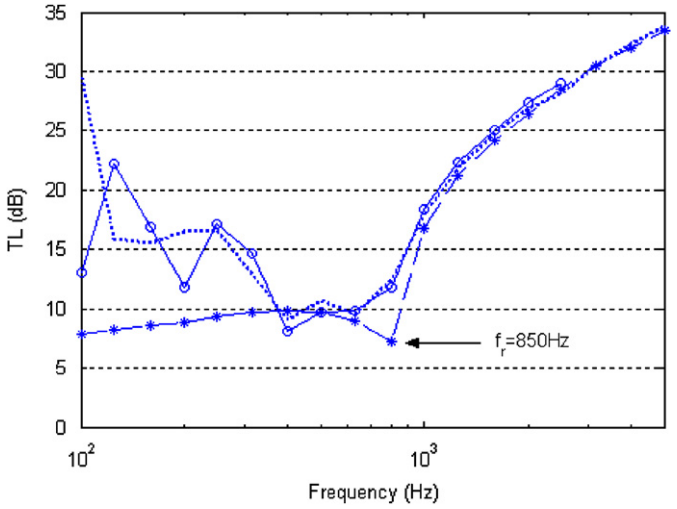

Fig. 14. Measured and predicted TL for Panel C: ------ Measurement; —○— Cal., clamped; ---*--- Cal., infinite model Ref. [3].

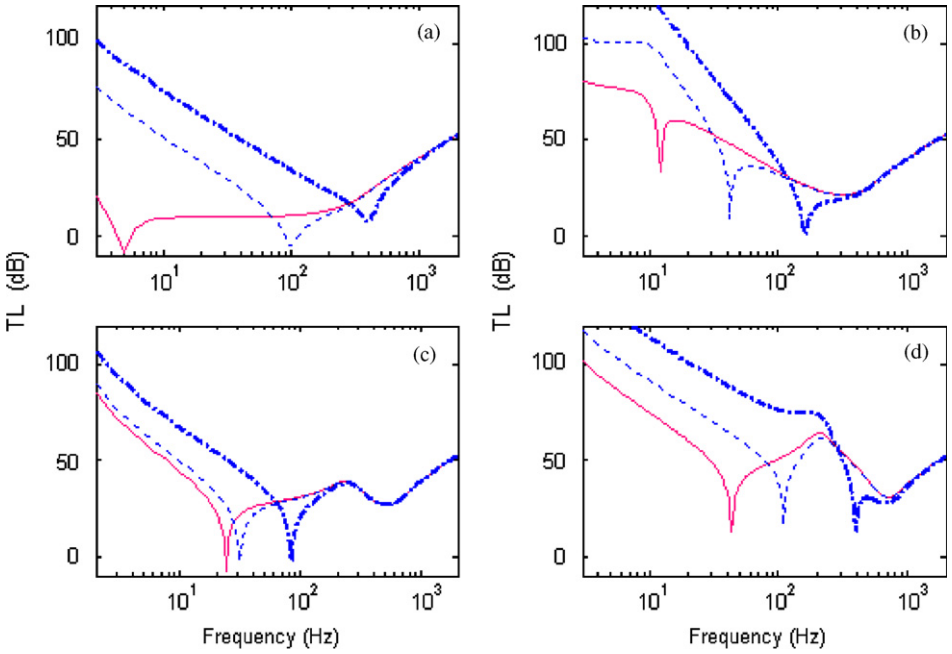

Fig. 15. Curvature influence on TL of individual mode: (a) mode (1,1); (b) mode (1,2); (c) mode (1,3); (d) mode (3,3). —— Panel A, flat; ------- Panel B, $r = 4$; ▬▬▬ Panel C, $r = 1$.

The reason that the curvature reduces sound transmission loss near ring frequencies is caused by convergence of resonance frequencies of the panel led by the interaction of bending forces and membrane forces in the shell. The convergence not only increases the modal density of the curved panel around the ring frequency, but also increases the sound radiation efficiency of these modes by shifting them to a relatively higher frequency. For example, the mode (1,1) of panel A is only a few Hertz, but this mode for panel C is about 400 Hz. Fig. 15 shows examples of the sound transmission loss of individual modes of the panel with different curvature, where the shift of resonance frequencies on sound transmission loss are evident.

For a curved, finite panel, the resonances shift from lower frequencies to higher frequencies but will never exceed the ring frequency of a corresponding full cylinder. For example, the resonance frequencies of mode

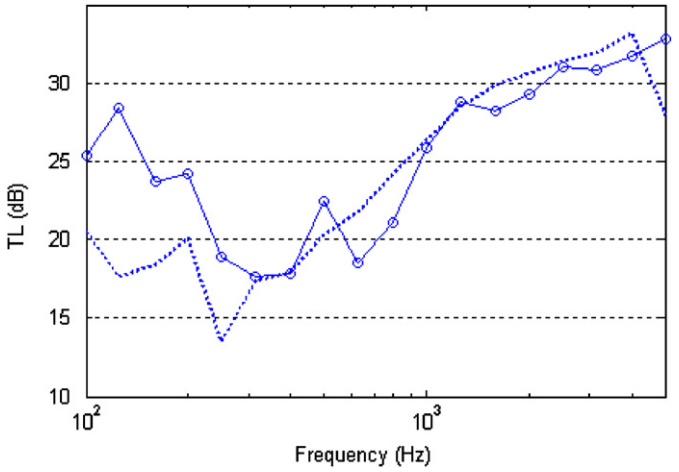

Fig. 16. Comparison of measured stringer influence on TL: ------ Panel E; —○— Panel F.

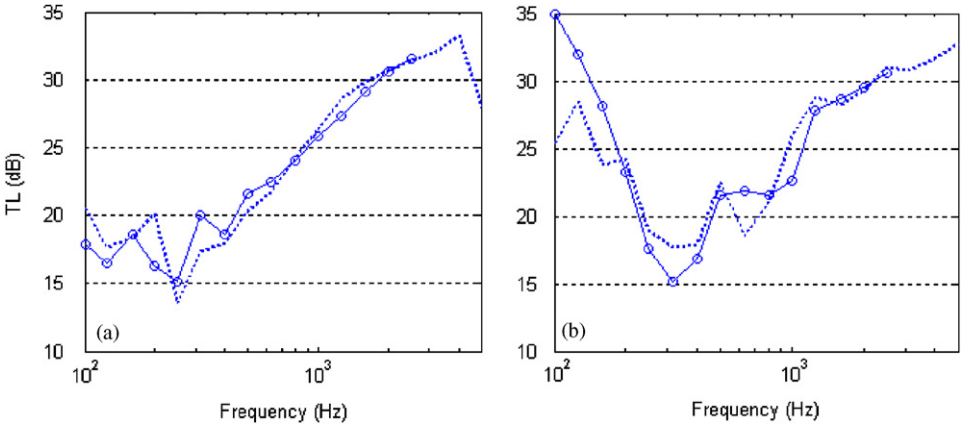

Fig. 17. Comparison of measured and predicted stringer influence on TL: (a) Panel E; (b) Panel F; ------ Cal.; —○— measurement.

(1,1) for panel B and C are about half of the corresponding ring frequencies, see Fig. 15 and also Eq. (17b). This explains that the least beneficial sound transmission loss measured and predicted by the finite models; located slightly below the ring frequency, rather than at the ring frequency as predicted by the infinite model.

3.1.2. Stiffener effect

The influences of stiffeners on the sound transmission of flat panel are shown in Figs. 16–17, where two small flat composite panels with and without stringers are tested and calculated. Figs. 16 and 17 indicate clearly that the stringers improve sound transmission loss at low frequencies, whilst significant deterioration is observed at relatively high frequencies. The behavior can be well explained by the effect of introduced low wavenumber components due to boundaries or stiffening, which then subsequently increases the radiation efficiency below the critical frequency [12]. In practice it may seem frustrating for the designer to observe no great improvement of sound insulation even with extra damping and increased mass due to the additional stringers.

The predictive techniques follow the trends in the measurements for the stiffened panel for most of the frequency range, Fig. 17. The discrepancies between measurement and prediction below 200 Hz may be due to the small panel size, uncertain panel boundary condition or the unconstrained boundary of the stringers at both ends in the measurement. There is some evidence from the vibro-acoustic tests showing that the stringer

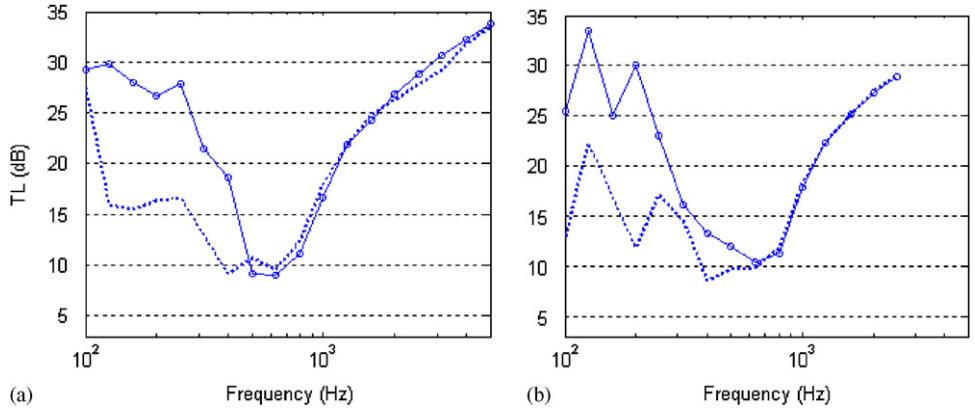

Fig. 18. Comparison of ring stiffener influence on TL: (a) measurement; (b) calculation; - - - - - - Panel C; —○— Panel D.

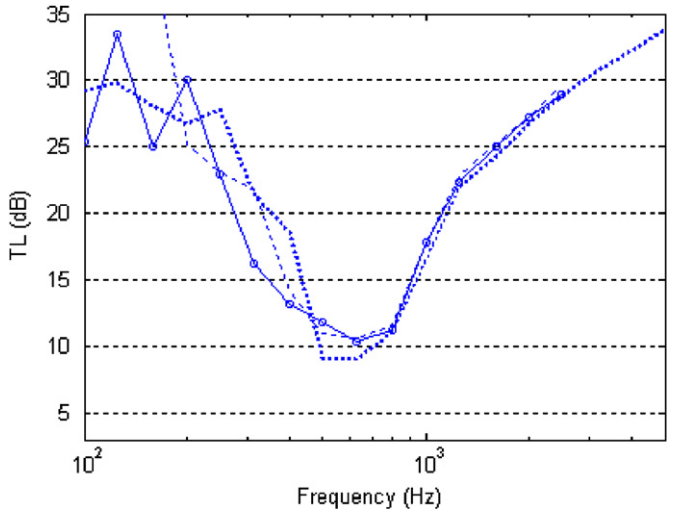

Fig. 19. Comparison of measured and predicted TL for Panel D: ▬▬▬ measurement; —○— cal., stiffening model; - - - - - - cal., subpanel model.

itself may play a role on sound radiation. Such effects, however, are not covered in this article but are worth further investigation.

The effects of circumferential stiffener on sound transmission loss are shown in Fig. 18–19, where two curved panels with and without ring ribs are measured and calculated. From the test and theoretical prediction, it is evident that the ribs considerably increase sound transmission loss far below the ring frequency, while no significant influence on sound transmission loss around and above the ring frequency. Above the ring frequency, the prediction agrees well with that of measurement, and below there are some deviations. The deviations are tolerable if one is willing to consider that Panel D has wide stiffeners, which may cause errors in calculation due to the line receptance assumption.

Because the stiffener is very heavy and stiff in comparison with the skin panel, it is expected that the sub-panels between two stiffeners may behave independently of each other as frequency increases. The sound transmission loss of the individual sub panel between two stiffeners is also calculated and shown in Fig. 19. For the case studied, it is clear that the sub-panel model and the stiffening model give similar results above 400 Hz, but for frequencies below 200 Hz, the sub-panel model failed to give an accurate prediction. For the sound transmission loss calculation, this example shows that the ring-stiffened panel can be modelled by a sub-panel between two stiffeners in most frequency ranges if the rib is stiff enough. Compared with the stiffening model, the sub-panel model, of course, is much simpler and requires much less calculation time.

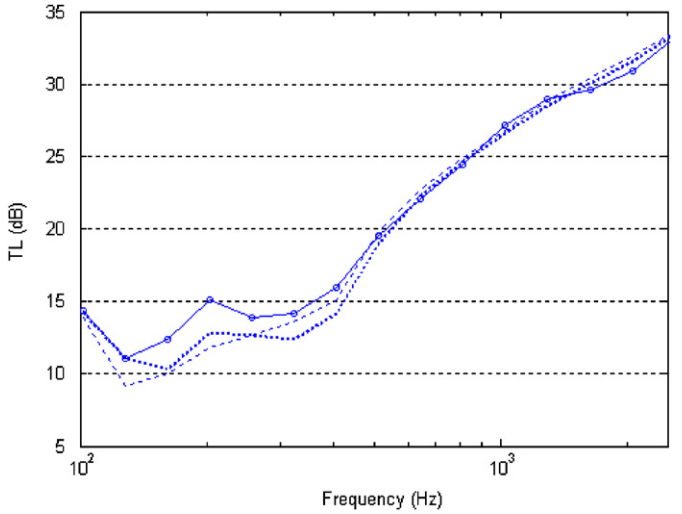

Fig. 20. Comparison of predicted TL for Panel G by using different model: ▬▬▬ skin only; - - - - - - skin + ring frames; —○— skin + axial stringers, $f_r \approx 420$ Hz.

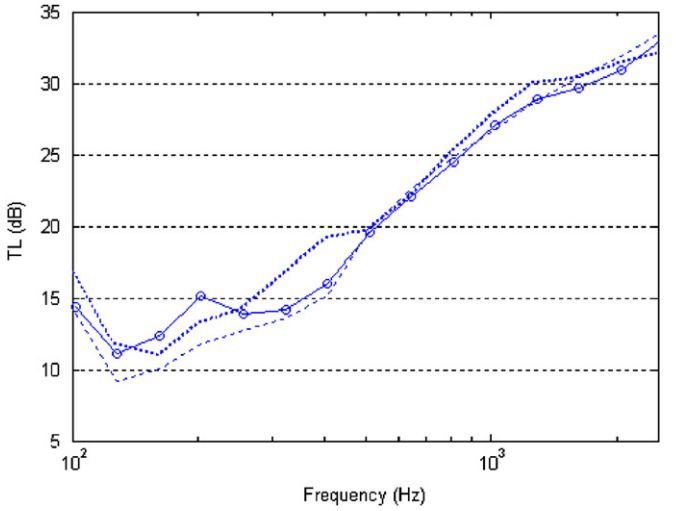

Fig. 21. Comparison of measured and predicted TL for Panel G: ▬▬▬ measurement; - - - - - - cal., skin + ring frames; —○— cal., skin + axial stringers.

3.1.3. *Comparison of the panels with both stringers and ring frames*

Comparison of measured and predicted sound transmission loss for the curved, large aircraft panels (Panels G and Panel H) are shown in Figs. 20–23. The study of these panels is the main purpose of this investigation. The ring frequency and the skin critical frequency are approximate 420 and 5700 Hz for Panel G; whilst, respectively, 410 and 3700 Hz for Panel H. Three models, viz., isotropic skin model, skin + ring frames model and skin + stringers model, are calculated and compared with corresponding measurements. The model of curved panel with both ring frames and stringers gives results similar to those predicted by the model of curved panel with stringers only, but cost increased computational time, therefore the calculation from the model of curved panel with both ring frames and stringer is not presented in this paper.

When compared with the prediction from the isotropic panel skin model, Figs. 20 and 22 show that the ring stiffeners only have little influence on sound transmission loss below 400 Hz, and have no effect above. The

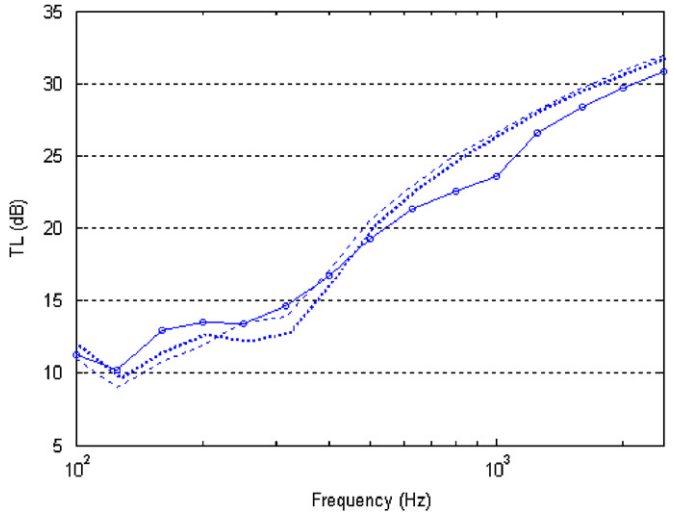

Fig. 22. Comparison of predicted TL for Panel H by using different model: ▬▬▬ skin only; ------ skin + ring frames; —○— skin + axial stringers, $f_r \approx 410$ Hz.

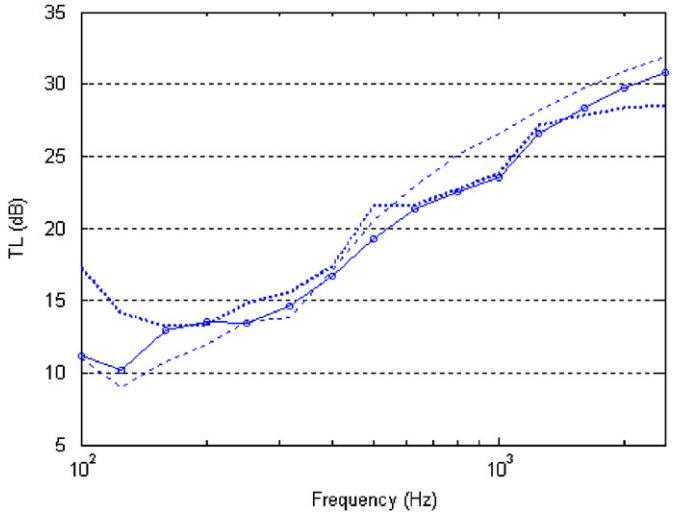

Fig. 23. Comparison of predicted and measured TL for Panel H: ▬▬▬ measurement;cal., ------ skin + ring frames; —○— cal., skin + axial stringers.

reason may be result from the sparsely-arranged ring frames for Panels G and H. Unlike ring frames, the axial stiffeners slightly improve sound transmission loss below 400 Hz, see Figs. 20 and 22, and above 400 Hz, the stringer effects for the metallic panel are not evident (Fig. 20), but for the composite panel, the deterioration of sound transmission loss near 1 kHz is obvious (Fig. 22).

As the ring stiffeners almost have no effect in the frequency range of interest, it is expected that the skin/stringer model is valid in describing the sound transmission behavior for the aircraft panel. Figs. 21 and 23 clearly show that the skin/stringer model improves the isotropic skin panel model by agreeing well with measurement data in the frequency range of interest. The discrepancies between measured and predicted sound transmission loss for Panel H at rather lower frequency may result from the isotropic assumption in the calculation. For Panel H, the measured Young's modulus shows there is a kind of orthotropic nature in the axial and circumferential direction, but in calculations, this effect is not included.

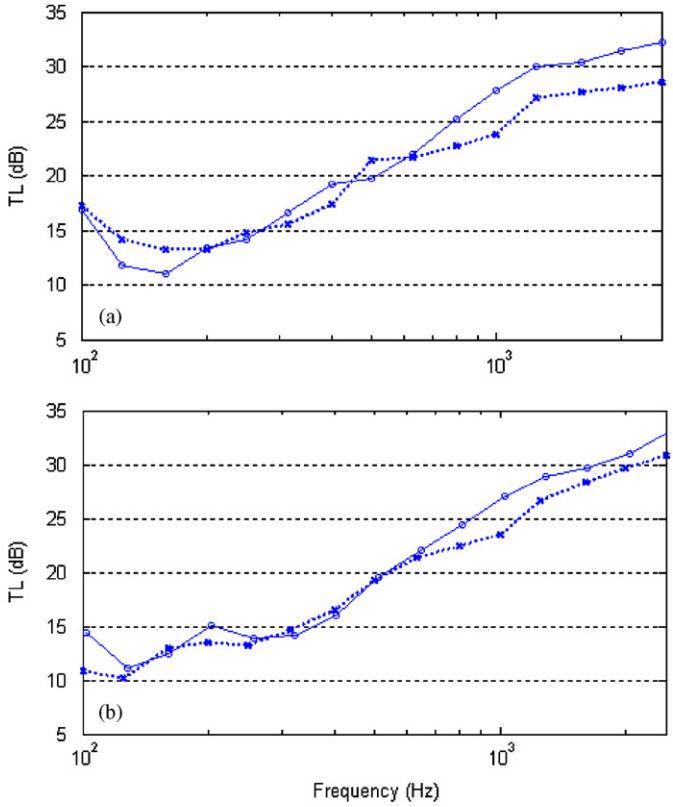

Fig. 24. Comparison of measured and predicted TL for Panel G and Panel H: (a) measurement; (b) prediction; —○— Panel G; - - -∗- - - Panel H.

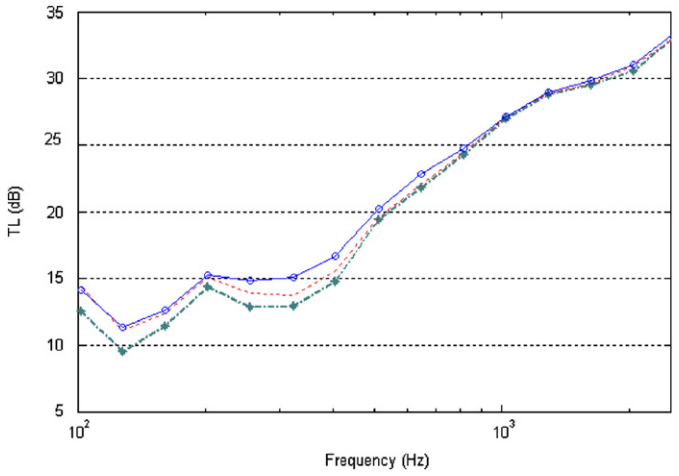

Fig. 25. Predicted skin loss factor influence on sound transmission loss: —○— skin loss factor 10%; - - - - - - skin loss factor same as Table 2; ------ ∗ ------ skin loss factor 1%. The stringer loss factor 1.5%, Panel G, $f_r \approx 420$ Hz.

In comparing the metallic panel with the same weight composite panel, Fig. 24, both measurement and prediction indicate that sound insulation properties of the composite panel are not as beneficial as that of the metallic panel in the frequency range. As mentioned above, the composite stringers attached to the composite panel play a role in this reduction, see Fig. 23.

As an example, the influence of skin loss factor on sound transmission loss is shown in Fig. 25. The numerical results reveal that increasing skin loss factor from 1% to 10% increases sound transmission loss about 1–2 dB below 500 Hz. In this frequency range, the sound transmission is dominant by resonance transmission due to modal convergence and higher radiation efficiency led by curvature. At frequencies above twice the corresponding ring frequency and but still well below the critical frequency, it is expected that the influence of skin loss factor is not significant because the sound transmission is dominated by forced transmission.

4. Further numerical investigation of stringer effects

Since the stringers may have potential deterioration on sound transmission loss through curved panels at relatively higher frequencies, it is of interest to see how stringer parameters affect sound transmission loss. Table 4 shows the panels used in numerical simulation for this purpose. In Table 4, Panels I1 and I2 are aluminum panels, with same size and surface density but with different curvature; Panels J1 and J2 are composites panels with same weight. The stringers attached to the panels are assumed rectangular cross-section and same weight, Table 5. The stringers are equally spaced.

For the panels studied, Fig. 26 shows that the stringers reduce sound transmission loss above 400 Hz for the composite panels and the aluminum panels, with and without curvature. At frequencies below 400 Hz, the stringers slightly increase sound transmission loss for the curved panels, Fig. 26(c)(d), but not the flat panels, Fig. 26(a)(b).

From Fig. 26, it is of interest to note that the stringer influence on composite panel is much larger than that of the aluminum panel. It is evident that the sound transmission loss for composite panels with composite stringers are much lower than that of aluminum panel with aluminum stringers, both being lower than that of the flat panels. Such results are also validated by measurements which have been partially presented in Section 2. For the flat panels studied, however, there is no significant difference of the sound transmission loss between the composite panel and the aluminum panel for frequencies up to 2500 Hz.

The comparison of the stringer cross-section shape on sound transmission loss is shown in Figs. 27–28, where the stringers with the same weight but different cross-section thickness and height are investigated. It is of interest to note that the lower height cross-section of the stringer, the lower negative effect on sound transmission loss in the frequency range is calculated. It seems that the short and wide cross-section of the stringer reduces the curvature effect of a curved panel and may liken it to behavior more like a flat uniform panel. The effect of cross-section shape on sound transmission loss, however, is not linear, which suggests that an optimization design for the stringers is necessary to improve airborne insulation properties for aircraft panels.

Table 4
Panels used in calculation

Panel	Radius (m)	Size (m^2)	Skin area density (kg/m^3)	Young's modulus (N/m^2)	Loss factor
I1	∞	1.1×1.162	5.4	6.85E + 10	Same as panel G
I2	2	1.1×1.162	5.4	6.85E + 10	
J1	∞	1.1×1.162	5.4	3.25E + 10	Same as panel H
J2	2	1.1×1.162	5.4	3.25E + 10	

Table 5
Stringers attached to the panels used in calculation

Panel	Material	Thickness (mm)	Height (mm)	Density (kg/m^3)	Young's modulus (N/m^2)	Stiffener Number	Loss factor
I1, I2	Aluminum	1.5	30	2700	6.85E + 10	6	0.015
J1, J2	Composite	2	38	1620	3.25E + 10	6	

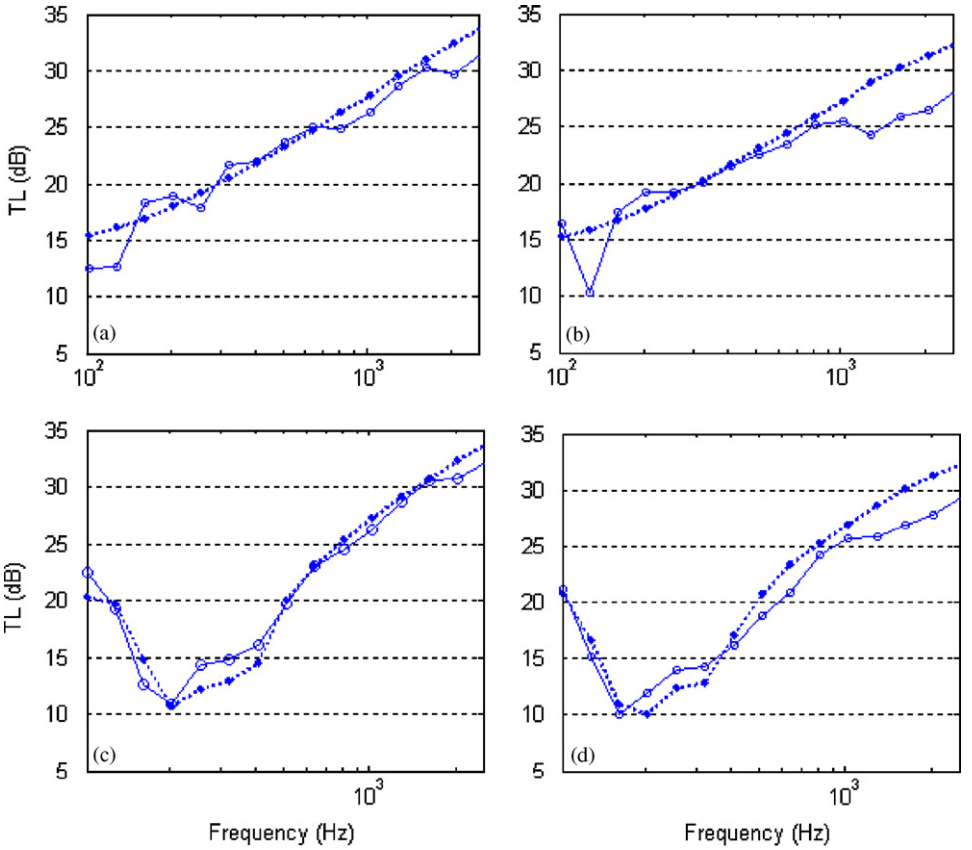

Fig. 26. Predicted stringer influences on sound transmission loss: (a) Panel I1, aluminum flat panel; (b) Panel J1, composite flat panel; (c) Panel I2, aluminum curved panel; (d) Panel J2, composite curved panel. ---*--- skin only; —○— skin with stringer attachments.

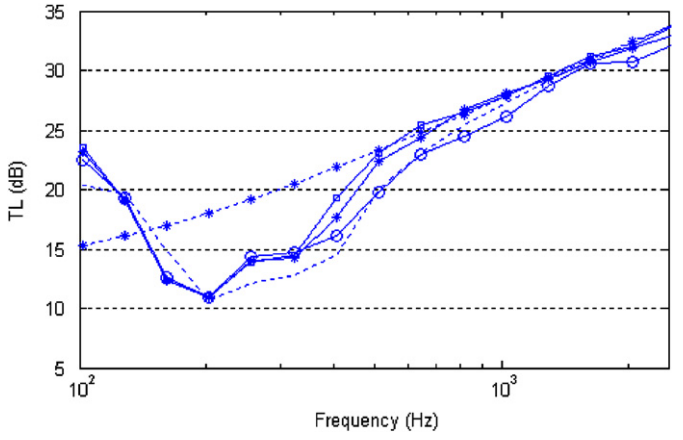

Fig. 27. Predicted stringer cross-section influences on sound transmission loss of aluminum panel: ---*--- flat skin only; ------ curved skin only; ---□--- skin with stringer attachments (6 mm × 7.5 mm); —*— skin with stringer attachments (3 mm × 15 mm); —○— skin with stringer attachments (1.5 mm × 30 mm); Panel I.

5. Concluding remarks

A numerical approach based on receptance method has been developed in this article to evaluate the airborne sound insulation of curved aircraft panels with stringer and ring frame attachments. Experimental

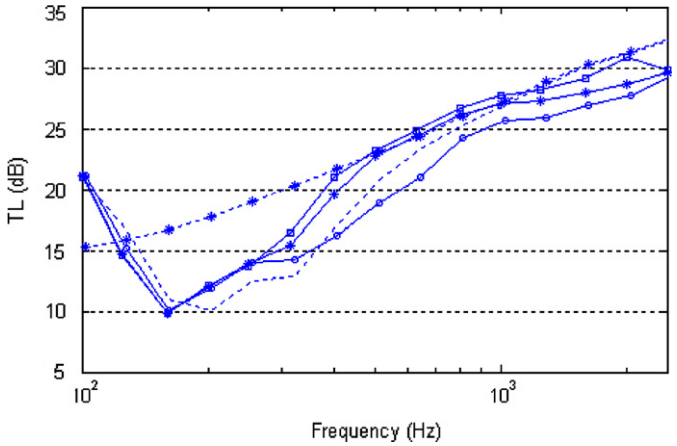

Fig. 28. Predicted stringer cross-section influences on sound transmission loss of composite panel: ---*--- flat skin only; ------ curved skin only; —□— skin with stringer attachments (12 mm × 9.5 mm); —*— skin with stringer attachments (6 mm × 19 mm); —○— skin with stringer attachments (3 mm × 38 mm); Panel J.

data for laboratory panels and aircraft panels have been collected by laboratory measurement. Theoretical predictions agree well with the test results in most frequency ranges of interest.

It was found that a small curvature may result in significant deterioration of the sound transmission loss at frequencies of interest. Unlike a flat uniform panel, the prediction for curved panels from the infinite model can not provide good agreement with the measurement close to and well below the ring frequency. However, in this frequency range, the finite model has been proved to be applicable.

For large curved aircraft panels studied here, it was found that the ring frames have little influence on sound transmission loss in the frequency range of interest. The reason results from the sparsely-arranged ring frames in practical situation. Compared with the ring frames, the stringers may have significant influence on sound transmission loss. It is evident that the stringer will slightly improve sound transmission loss of a curved panel around the ring frequency, but it may result in potential deterioration of sound transmission loss above the ring frequency. It is of interest to note that the sound transmission loss of the composite skin panel attached with composite stringers is much lower than that of the metallic skin panel attached with metallic stringers. The relatively high cross-section of the stringer may be a reason for this behaviour.

The theoretical approach presented in this article may provide a way for the acoustical optimization design of stringers to improve airborne sound insulation for aircraft panels. The work may also be extended by including the influence of the acoustical radiation of the stringers on sound transmission loss and is currently underway.

Acknowledgements

The authors gratefully acknowledge the constructive technique support by Kent Lindgren and Danilo Prelevic, useful discussion with Dr. Andrew Peplow in MWL, and the financial support by EU project, Friendly Aircraft Cabin Environment.

Appendix A:

From Eqs. (10) and (36), the transmitted power for the curved panel with stinger attachments may be calculated by

$$\Pi^t = \frac{1}{2}\rho_0 c_0 \sum_{mn} \sigma_{mn} |V_{mn}|^2 = \frac{1}{2}\rho_0 c_0 \sum_{mn} \sigma_{mn} \left| Y_{c,mn} \right|^2 \left| P^i_{mn} - \sum_{n'} P^i_{mn'} Y_{c,mn'} \mathbf{\Phi}_{n'} \right|^2 . \tag{A.1}$$

Expanding Eq. (A1) and neglecting the cross terms of $P^i_{mn}P^i_{m'n'}$ since the average of them over all incident angles is related to the cross terms of modal radiation efficiency, one may have

$$\Pi^t = \frac{1}{2}\rho_0 c_0 \sum_{mn} \sigma_{mn} \left| Y_{c,mn} \right|^2 \left(\left| P^i_{mn} \right|^2 - 2 \left| P^i_{mn} \right|^2 \mathrm{Re}\left\{ Y_{c,mn} \mathbf{\Phi}_n \right\} + \sum_{n'} \left| P^i_{mn'} \right|^2 \left| Y_{c,mn'} \mathbf{\Phi}_{n'} \right|^2 \right). \tag{A.2}$$

By employing the similar procedure used in Eqs. (11), (12) and (13), the expression for sound transmission loss through the curved panel with stringer attachments is obtained in Eq. (38).

References

[1] P.W. Smith, Sound Transmission through thin cylindrical shell, *Journal of the Acoustical Society of America* 29 (1957) 721–729.

[2] L.R. Koval, On sound transmission into a thin cylindrical shell under "flight conditions", *Journal of Sound and Vibration* 48 (1976) 265–275.

[3] L.R. Koval, Effect of air flow, panel curvature, and internal pressurization on field-incidence transmission loss, *Journal of the Acoustical Society of America* 59 (1976) 1379–1385.

[4] L.R. Koval, Effects of cavity resonances on sound transmission into a thin cylindrical shell, *Journal of Sound and Vibration* 59 (1978) 23–33.

[5] L.R. Koval, On sound transmission into an orthotropic shell, *Journal of Sound and Vibration* 63 (1979) 51–59.

[6] L.R. Koval, Effects of longitudinal stringers on sound transmission into a thin cylindrical shell, *Journal of Aircraft* 15 (1978) 816–821.

[7] L.R. Koval, On sound transmission into a stiffened cylindrical shell with rings and stringers treated as discrete elements, *Journal of Sound and Vibration* 71 (1980) 511–521.

[8] L.R. Koval, Sound transmission into a laminated composite cylindrical shell, *Journal of Sound and Vibration* 71 (1980) 523–530.

[9] A. Blaise, C. Lesueur, M. Gotteland, M. Barbe, On sound transmission into an orthotropic infinite shell: comparison with Koval's results and understanding of phenomena, *Journal of Sound and Vibration* 159 (1991) 233–243.

[10] C. Lesueur, *Rayonnement Acoustique Des Structures- Vibroacoustique-Interactions Fluide Structure*, Collection EDF-DER, Editions Eyroolles, Paris, 1988.

[11] B. Liu, L. Feng, Sound transmission through a double-walled cylindrical shell, *Proceedings of the 10th International Congress on Sound and Vibration*, KTH, Stockholm, Sweden, July, 2003, pp. 4617–4624.

[12] F. Fahy, *Sound and Structural Vibration: Radiation, Transmission and Response*, Academic Press, London, 1985.

[13] J.-H. Lee, J. Kim, Sound transmission through periodically stiffened cylindrical shells, *Journal of Sound and Vibration* 251 (2002) 431–456.

[14] I.D. Wilken, W. Soedel, The receptance method applied to ring stiffened cylindrical shells: analysis of modal characteristics, *Journal of Sound and Vibration* 44 (1976) 563–576.

[15] I.D. Wilken, W. Soedel, Simplified prediction of the modal characteristics of ring-stiffened cylindrical shells, *Journal of Sound and Vibration* 44 (1976) 577–589.

[16] T. Lin, Wave motion in finite coupled structures, with application to ship structures, Ph.D Thesis, the University of Western Australia, 2005.

[17] J.H. Lee, J.G. Ih, Significance of resonant sound transmission in finite single partitions, *Journal of Sound and Vibration* 277 (2004) 881–893.

[18] D. Takahashi, Effects of panel boundedness on sound transmission problems, *Journal of the Acoustical Society of America* 98 (1995) 2598–2606.

[19] W.L. Li, H.J. Gibeling, Determination of the mutual radiation efficiencies of a rectangular plate and their impact on the radiated sound power, *Journal of Sound and Vibration* 229 (2000) 1213–1233.

[20] C.E. Wallace, Radiation resistance of a rectangular panel, *Journal of the Acoustical Society of America* 51 (1972) 947–952.

[21] A.K. Mitchell, C.R. Hazell, A simple frequency formula for clamped rectangular plates, *Journal of Sound and Vibration* 118 (1987) 271–281.

[22] W. Soedel, *Vibrations of Shells and Plates*, Marcel Dekker, New York, 1981.

[23] B. Liu, Influence of baffle size and curvature on sound radiated by vibrating panels, *Proceedings of the 11th International Congress on Sound and Vibration*, St-Petersburg, Russia, July, 2004, pp. 1871–1878.

[24] S. Timoshenko, D.H. Young, W. Weaver Jr., *Vibration Problems in Engineering*, Wiley, New York, 1974.

[25] T. Wah, Flexural vibrations of ring-stiffened cylindrical shells, *Journal of Sound and Vibration* 3 (1966) 242–251.

[26] ISO 15186-1:2000 Acoustics—measurement of sound insulation in buildings and of building elements using sound intensity—part 1: Laboratory measurements.